Estuaries and Coasts (2015) 38 (Suppl 1):S187–S202
DOI 10.1007/s12237-013-9684-2

Modeling the Effects of Tidal Energy Extraction on Estuarine Hydrodynamics in a Stratified Estuary

Zhaoqing Yang · Taiping Wang

Received: 7 July 2012 / Revised: 11 July 2013 / Accepted: 19 July 2013 / Published online: 15 August 2013
© Coastal and Estuarine Research Federation 2013

Abstract A 3-D coastal ocean model with a tidal turbine module was used in this paper to study the effects of tidal energy extraction on temperature and salinity stratification and density-driven two-layer estuarine circulation. Numerical experiments with various turbine array configurations were carried out to investigate the changes in tidally averaged temperature, salinity, and velocity profiles in an idealized stratified estuary that connects to coastal water through a narrow tidal channel. The model was driven by tides, river inflow, and sea surface heat flux. To represent the realistic size of commercial tidal farms, model simulations were conducted based on a small percentage (less than 10 %) of the total number of turbines that would generate the maximum extractable energy in the system. Model results show that extraction of tidal in-stream energy will increase the vertical mixing and decrease the stratification in the estuary. Installation of in-stream tidal farm will cause a phase lag in tidal wave, which leads to large differences in tidal currents between baseline and tidal farm conditions. Extraction of tidal energy in an estuarine system has stronger impact on the tidally averaged salinity, temperature, and velocity in the surface layer than the bottom layer even though the turbine hub height is close to the bottom. Finally, model results also indicate that extraction of tidal energy weakens the two-layer estuarine circulation, especially during neap tides when tidal mixing is weakest and energy extraction is smallest.

Keywords Tidal stream energy · Numerical modeling · Vertical mixing · Stratification · Estuarine circulation

Communicated by Gayle Zydlewski

Z. Yang (✉) · T. Wang
Pacific Northwest National Laboratory, 1100 Dexter Ave North, Ste 400, Seattle, WA 98109, USA
e-mail: zhaoqing.yang@pnnl.gov

Introduction

There have been rapid developments seeking renewable energy alternatives due to the growing concerns of climate change and strong demand of global reduction of greenhouse effect due to human energy consumption. Harnessing in-stream tidal energy gains much attention because of the high predictability, and oftentimes, the energy resources are close to the coastal regions with high population. In recent years, many studies have been conducted to assess the maximum extractable tidal energy using numerical models and analytical methods. For example, Garrett and Cummins (2004, 2005, 2008) and Blanchfield et al. (2008) developed a simple theoretical model to estimate the upper limit of the extractable tidal energy in a tidal channel connecting to a basin as a function of tidal amplitude and the maximum undisturbed volume flux through the channel. These analytical studies provided fundamental understanding and insight to the dynamics of tidal energy extraction in a simplified tidal system. However, for more detailed and site-specific analysis, analytical models are often limited because of the underlined assumptions and simplifications.

Numerical models have been widely used to assess in-stream tidal energy resources and evaluate impacts of tidal energy extraction on hydrodynamics and marine environments. These modeling studies range from 1-D to 3-D models at laboratory scale to a real-world site. Sun et al. (2008) evaluated the local effects of tidal energy extraction on the flow field at a laboratory scale using a computational fluid dynamics code. Walkington and Burrows (2009) simulated the tidal stream power potential and impacts of installed tidal farm capacity on the west coast of the UK using a depth-averaged 2-D model. Draper et al. (2009) also used a 2-D model to investigate the effects of tidal energy extraction on tidal hydrodynamics in a simple tidal channel. With the rapid growth of computation resource, 3-D models have been used to simulate the potential of tidal energy extraction and its

environmental effect. Shapiro (2010) applied a 3-D ocean circulation model to study the effects of tidal energy extraction on tidal current magnitudes and transport process in a shallow sea. Defne et al. (2011) modeled the effects of tidal power extraction on the estuarine hydrodynamics along the Georgia coast using the 3-D Regional Ocean Modeling System. Hasegawa et al. (2011) evaluated the far-field effects of tidal energy extraction in Minas Passage, Bay of Fundy, using a 3-D nested-grid modeling approach. More recently, Yang et al. (2013) implemented a tidal energy extraction module in the unstructured-grid Finite-Volume Coastal Ocean Model (FVCOM) to simulate the 3-D effects of tidal energy extraction in a channel linking to a bay system.

However, most of the studies related to environment impacts still primarily focus on the barotropic flow field, especially on the total volume flux across a large fence of tidal turbines. For example, Ahmadian et al. (2012) modeled the far-field hydro-environmental impacts, such as tidal currents, sediment, and fecal bacteria levels, due to the installation of tidal stream turbines in the Severn Estuary and Bristol Channel. Neill et al. (2009) applied a 1-D hydrodynamics and morphological model to evaluate the impacts of tidal energy extraction on the sediment dynamics in the Bristol Channel of the UK. Neill et al. (2012) further applied a 3-D model to simulate the impact of tidal energy converter arrays on the dynamic formation of headland sand banks in the Alderney Race. Furthermore, nearly all of the previous studies on the effects of tidal energy extraction on flow fields were conducted with the assumption of barotropic tidal motion, i.e., stratification and density-induced circulation were not considered. No studies have been found on evaluating the effects of tidal in-stream energy on estuarine stratification and two-layer baroclinic circulation. In reality, many hotspots with high tidal in-stream energy potential are often connected to estuaries with high freshwater discharge, which are subject to density stratification and baroclinic motion, such as the Admiralty Inlet and Tacoma Narrows of Puget Sound, USA. Stratification and estuarine two-layer circulation are important factors affecting the flushing time and biogeochemical processes in estuarine and coastal environments. In this study, the FVCOM model with tidal turbine module (Yang et al. 2013) was used to evaluate the effects of tidal energy extraction on the temperature and salinity stratification and the baroclinic two-layer circulation in an idealized estuary and bay system connected to the coastal ocean through a narrow channel.

Methods

Model Description and Model Domain

The 3-D unstructured-grid FVCOM with a tidal turbine module (Chen et al. 2003; Yang et al. 2013) was used in this study. FVCOM simulates water surface elevation, velocity, temperature, salinity, sediment, and water quality constituents. The unstructured-grid and finite-volume approach employed in the model provide geometric flexibility and computational efficiency that is well suited for simulating the tidal and estuarine circulations in estuaries and coastal bays. FVCOM uses unstructured triangular cells in the horizontal plane and a sigma-stretched coordinate system in the vertical direction to optimally represent the complex horizontal geometry and bottom topography. A mode splitting approach is used in the numerical scheme to solve the depth-averaged 2-D barotropic external mode and 3-D baroclinic internal mode equations. FVCOM has been used to simulate tidal and estuarine circulations (Huang et al. 2008; Xue et al. 2009; Yang and Khangaonkar 2010), storm surge and wave modeling (Weisberg and Zheng 2006; Qi et al. 2009), and nearshore restorations (Yang et al. 2010, 2011), as well as tidal energy extraction (Karsten et al. 2008; Yang et al. 2013).

To systematically evaluate the effect of tidal energy devices on flow field, an idealized model domain was developed, which is approximated with dimensions similar to Puget Sound, a tidally dominant fjord estuary in the Pacific Northwest, USA. The model domain consists of a semi-enclosed bay that is forced by the upstream river discharge and tidal forcing through a narrow tidal channel, which mimic the Puget Sound and Admiralty Inlet at its entrance (Fig. 1). The length of the tidal channel is 15,000 m, and the width is 30,000 m. The length of the tidal basin is 100,000 m, and the width is 20,000 m. The water depth in the channel and basin is 60 and 80 m, respectively. The dimensions of the tidal channel and bay system are shown in Table 1. The unstructured model grid consists of 25,415 elements and 13,148 nodes, with finer grid resolution in the tidal channel. The model cell size varies from 300 m in the tidal channel to around 4,500 m in the coastal ocean boundary. Twenty-one uniform sigma layers were specified in the water column for all model runs.

Model Forcing

To simulate temperature/salinity stratification and density-induced mean estuarine circulation, model forcing includes not only tide and river inflows, but also meteorological inputs. All forcing functions in this study were generated based on observed data in the Puget Sound region. To keep the tidal forcing simple but still representative of the spring and neap tidal cycle as observed in Puget Sound (Yang and Khangaonkar 2010), the principal lunar semidiurnal tide (M_2) with amplitude of 0.7 m and the principal solar semidiurnal tide (S_2) with amplitude of 0.3 m were specified along the open ocean boundary. In the upstream river boundary, river inflow and river temperature were specified. The river flow was idealized based on the climatology of total river inflow in Puget Sound. River inflow shows strong seasonal variations, with the highest

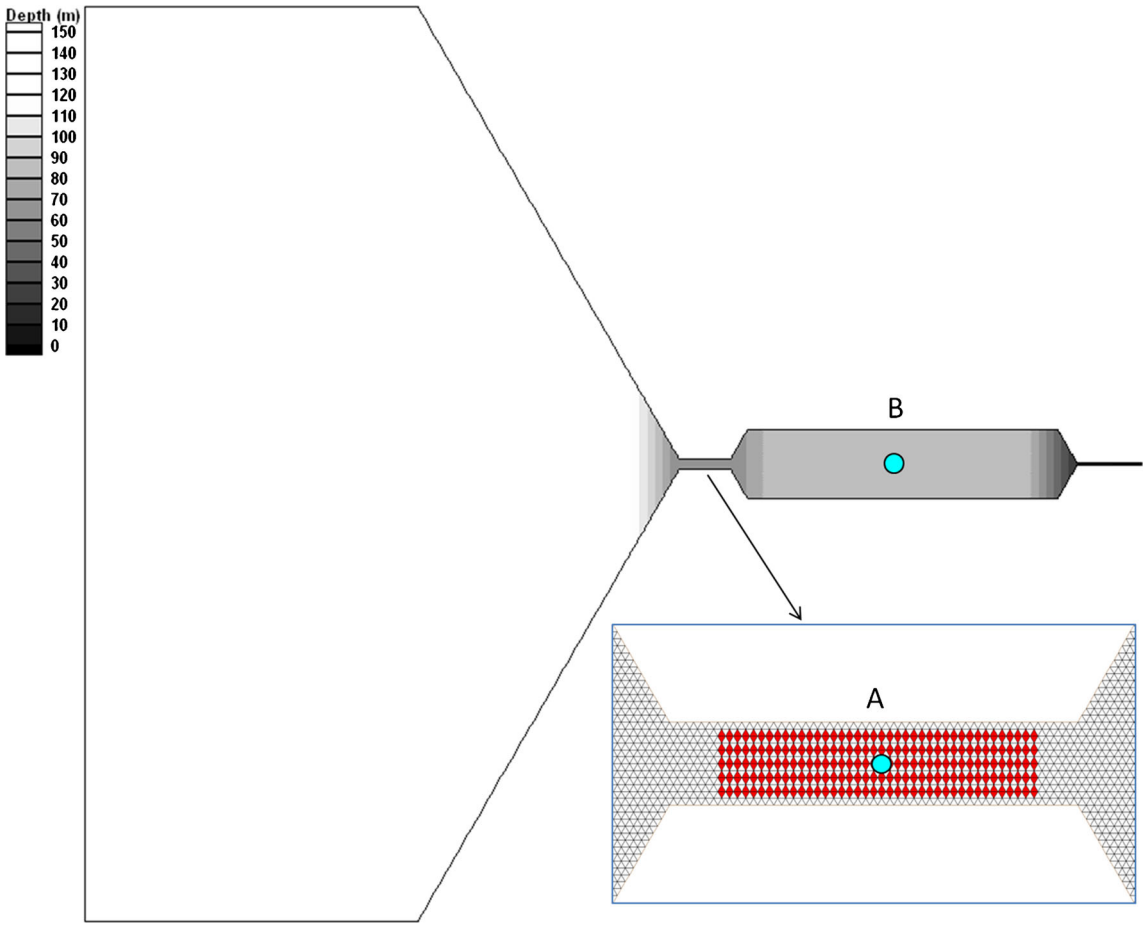

Fig. 1 Model domain and bathymetry—a tidal estuary connected to the coastal ocean through a narrow tidal channel. The *inset image* shows the unstructured model grid and array arrangement of 400 turbines in the tidal channel. *A* and *B* denote locations for profile and time series plots of model results

peak flow in December as a result of storms and floods. A second peak flow occurs in January, caused by the early snow melt, followed by a third peak due to spring snow melt. The lowest river flow (dry season) happens in September (Fig. 2a).

Long-term river temperature records in Puget Sound are very limited. Existing temperature measurements for the major rivers in Puget Sound showed relatively small to medium seasonal variations. The idealized river annual temperature distribution was developed based on 3 years of temperature records of Cedar River, which discharges into the main basin of Puget Sound. The annual temperature distribution basically follows a sinusoidal distribution pattern with a maximum temperature of 16 °C in July and a minimum temperature of 6 °C in January (Fig. 2b). Similarly, an annual sinusoidal distribution of air temperature with daily maximum and minimum variations was specified, based on measurements at the NOAA meteorological station at Seattle, Washington. The idealized daily maximum and minimum air temperatures as well as daily variations with comparison to the NOAA measured data are shown in Fig. 2c, d. For simplicity, short-term (weekly to monthly) fluctuations in air temperatures were filtered out.

Short- and long-wave solar radiations, sensible heat flux, latent heat flux, and the net heat flux are required for the prescribed meteorological forcing in FVCOM. Measurements for meteorological parameters in Puget Sound are very limited. To generate representative meteorological forcing, such as wind, solar radiation, and heat flux, we used hybrid data from Weather Forecast Research model prediction (http://www.wrf-

Table 1 Dimensions of the model domain

Tidal channel (m)			Semi-enclosed bay (m)			Coastal ocean (m)		
Length	Width	Depth	Length	Width	Depth	Length	Width	Depth
15,000	3,000	60	100,000	20,000	80	170,000	250,000	200

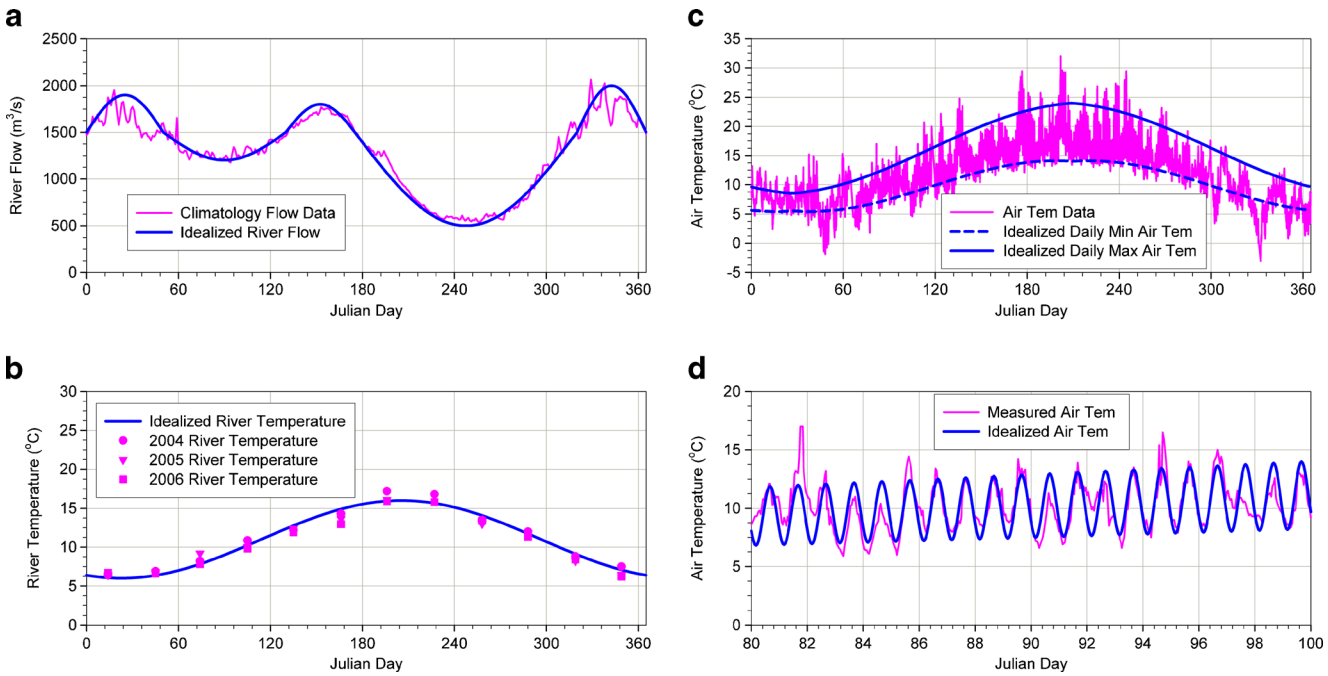

Fig. 2 Model inputs for river inflow (**a**), river temperature (**b**), and air temperature (**c**, **d**)

model.org/index.php) and NOAA measurements. The solar radiation was calculated based on the formula of a CE-QUAL-W2 model (Cole and Wells 2009). Details for calculation of net heat flux are given in Yang et al. (2010). The maximum solar radiation of 898 W/m^2 occurred in late June, and the minimum value of zero occurred at midnight daily (Fig. 3a, b). The maximum net heat flux is around 860 W/m^2 in late June, and the daily minimum net heat flux is −170 W/m^2, where the negative sign represents heat release from water to the atmosphere at night (Fig. 3c, d). Cloud cover data are very limited temporally, and cloud cover is not a major factor in heat exchange. Specification of temporally varying cloud cover with high uncertainty as model input does not necessarily provide better prediction of heat flux. Therefore, a constant cloud cover factor of 0.8 was used throughout the simulation period to account for the effect of cloud cover. Similarly, wind data are also limited, and wind pattern is very much site dependent. A constant westward wind speed of 2.5 m/s was considered for

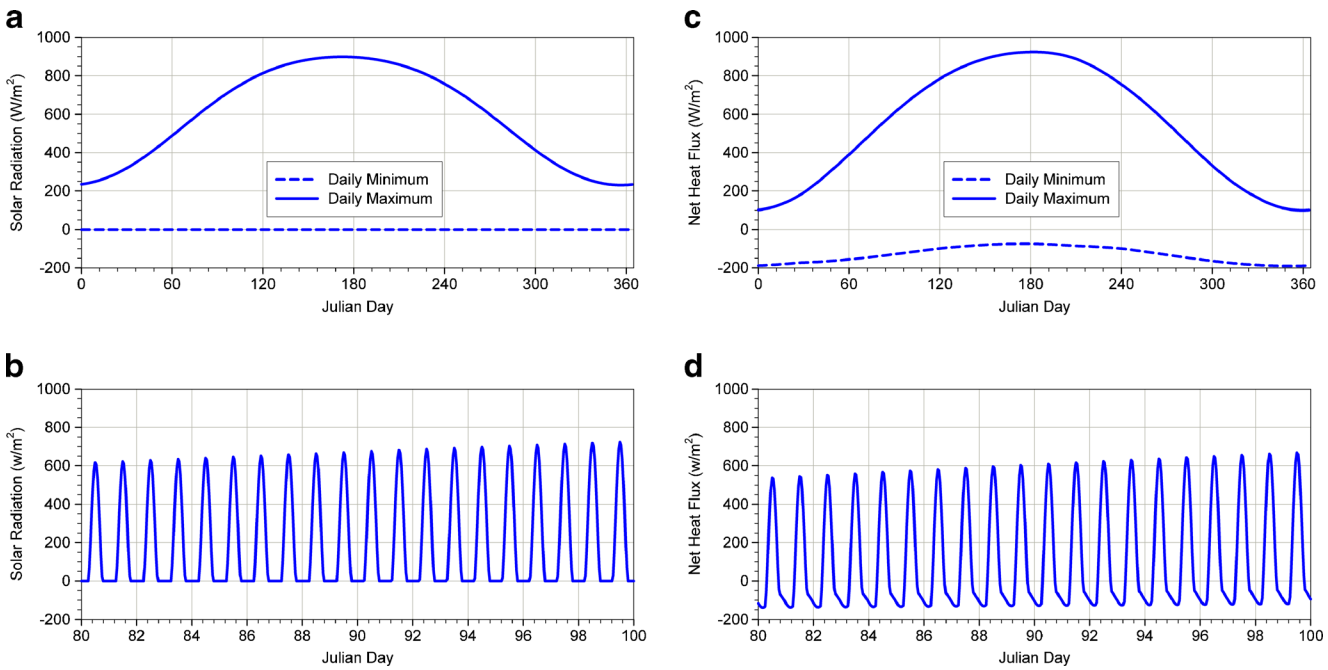

Fig. 3 Model inputs for solar radiation (**a**, **b**) and net heat flux (**c**, **d**)

the entire domain and simulation period. The tidal boundary condition was specified at every 15 min, and all river and meteorological inputs were specified in hourly intervals.

Modeling of Baseline Condition Without Tidal Turbines

To evaluate the effect of tidal energy extraction on the estuarine hydrodynamics in the tidal channel and bay system, a baseline condition without the presence of tidal turbines was first developed. To spin up the model, one full year simulation was conducted, and the model results were saved as a new initial condition for the new model run using the hot-start option. Time series of simulated tidal elevation and depth-averaged velocity in the tidal channel and bay are shown in Fig. 4. Strong semidiurnal tidal variations with spring and neap tidal cycle are seen in both tidal elevation and velocity distributions. Tidal range is amplified significantly in the semi-enclosed bay as tides propagate from the coastal ocean to the tidal basin, which is consistent to the tidal range distribution in Puget Sound (Yang and Wang 2013). Tidal velocity reaches its maximum in the narrow channel and becomes very small in the bay. Seasonal variations in tidal elevations and tidal velocities are negligible in the system.

Time series of surface and bottom salinities and temperatures in the tidal channel and the bay are shown in Fig. 5. There are strong stratifications in salinity and temperature distributions throughout the year. Surface salinity in the channel shows strong daily variation because of strong tidal exchange between the coastal seawater and freshwater from the estuary. There is also a clear seasonal pattern in surface salinity, with high surface salinity corresponding to low river discharge in late summer and low surface salinity corresponding to high river discharge in winter. Bottom salinity remains nearly constant, which is close to the salinity of coastal water outside of the channel. Surface temperature is mainly controlled by the surface heating from atmospheric forcing. Strong seasonal variations are observed in surface temperature distribution, which reaches the maximum during summer and turned over as water cooled from the surface in late fall and winter. Spring and neap tidal cycle signals are also clearly presented in both surface salinity and temperature distributions. Salinity and temperature in the bay show small daily variations but strong seasonal variations, similar to the channel.

Temperature/salinity and density stratifications and tidally averaged estuarine circulation are important factors affecting the biogeochemical processes in estuarine and coastal ecosystems. Time series of tidally averaged surface and bottom salinity, temperature, density anomaly, and velocity at location A in the tidal channel are shown in Fig. 6. There is a close correlation among the tidally averaged surface density anomaly and velocity (R^2=0.71), which shows strong modulation of the spring–neap tidal cycle at fortnightly frequency, with stronger outgoing surface currents occurring in neap tides. Low-pass-filtered (monthly) surface density anomaly and velocity also show a good correlation with R^2=0.79. It is well understood that water exchange and stratification are strongest at neap tides when tidal mixing become weakest. These results are consistent with previous studies on the dynamics of stratified estuaries (e.g., Geyer and Cannon 1982; Geyer et al. 2008; Murphy

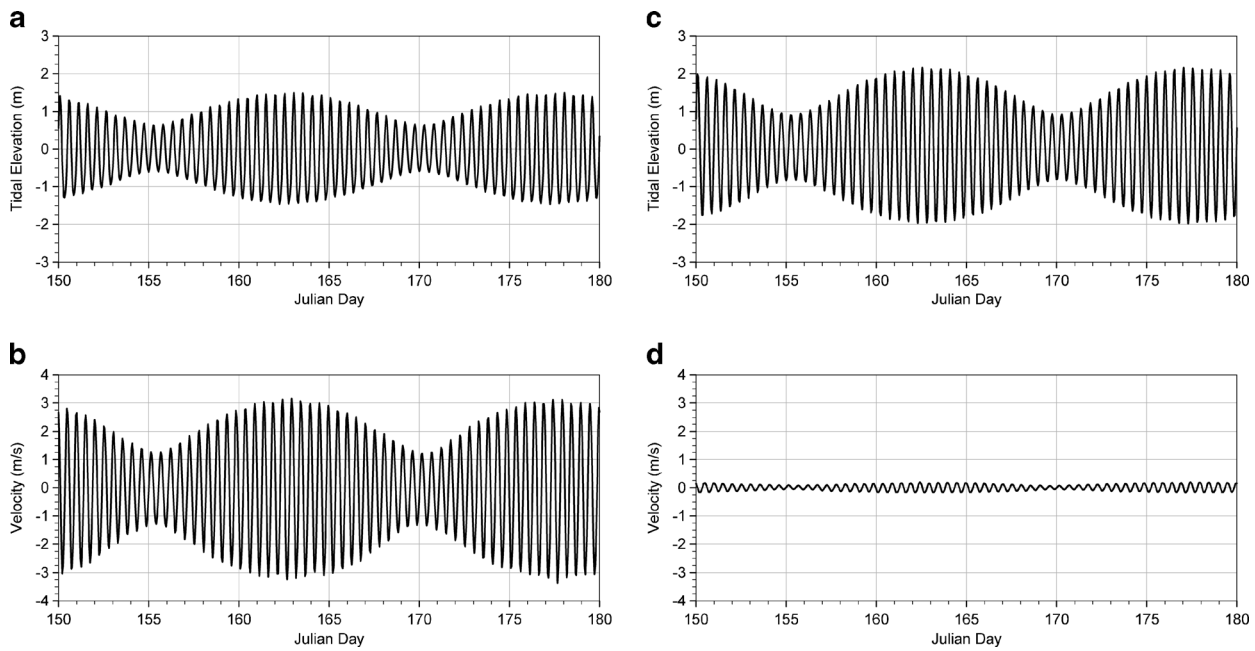

Fig. 4 Tidal elevations and depth-average velocities at location A in the tidal channel (**a**, **b**) and location B in the bay (**c**, **d**)

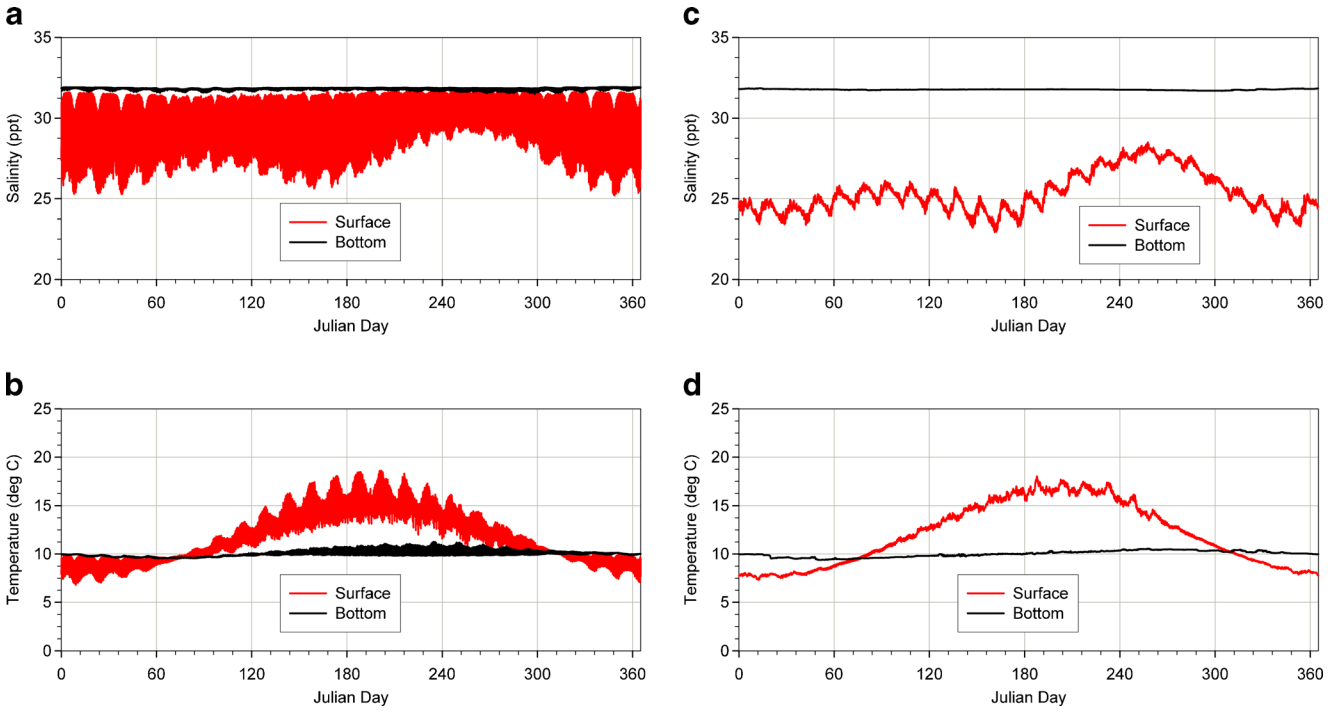

Fig. 5 Surface and bottom salinities and temperatures at location A in the tidal channel (**a**, **b**) and location B in the bay (**c**, **d**)

and Valle-Levinson 2008). Figure 6 also shows that the maximum mean surface current occurs in June (JD 150–165), corresponding to the high flow and warm season. To further examine the two-layer circulation pattern, tidally averaged temperature, salinity, and velocity profiles at spring and neap tides in the tidal channel are analyzed and shown in Fig. 7. Strong stratification is seen clearly in both salinity and temperature profiles. The two-layer estuarine circulation (negative velocity indicates current going out of the estuary) is well developed with stronger outgoing surface current during neap tide and weaker outgoing surface current during spring tide.

Model Applications to Tidal Energy Extraction

Maximum Extractable Tidal Energy in Baroclinic Mode

To simulate the effect of tidal energy extraction, a momentum sink approach is used in this study. The momentum governing equations for Reynolds-averaged turbulent flows with momentum sink terms due to energy extraction have the following general form:

$$\frac{\partial u}{\partial t}+u\frac{\partial u}{\partial x}+v\frac{\partial u}{\partial y}+w\frac{\partial u}{\partial z}-fv = -\frac{1}{\rho_o}\frac{\partial p}{\partial x}+\frac{\partial}{\partial z}\left(K_m\frac{\partial u}{\partial z}\right)+F_x-F_x^M \quad (1)$$

$$\frac{\partial v}{\partial t}+u\frac{\partial v}{\partial x}+v\frac{\partial v}{\partial y}+w\frac{\partial v}{\partial z}-fu = -\frac{1}{\rho_o}\frac{\partial p}{\partial y}+\frac{\partial}{\partial z}\left(K_m\frac{\partial v}{\partial z}\right)+F_y-F_y^M \quad (2)$$

where (x, y, z) are the east, north, and vertical axes in the Cartesian coordinates; (u, v, w) are the three velocity components in the x, y, and z directions; (F_x, F_y) are the horizontal momentum diffusivity terms in the x and y directions; K_m is the vertical eddy viscosity coefficient; ρ is water density; p is pressure; and f is the Coriolis parameter. $\overrightarrow{F^M}=\left(F_x^M, F_y^M\right)$ are the added momentum sink terms corresponding to energy extraction that can be defined as follows:

$$\overrightarrow{F^M}=\frac{1}{2}\frac{C_e A}{V_c}\left|\overrightarrow{u}\right|\overrightarrow{u} \quad (3)$$

where V_c is a control volume, C_e is momentum extraction coefficient which takes into account for the rotor blade thrust and the drag of turbine structure, A is the flow-facing area of the turbines, and $\overrightarrow{u}$ is the velocity vector. FVCOM solves the momentum governing equations using a finite-volume method and sigma-stretch coordinate transformation in the vertical direction. Details on the numerical method for solving Eq. (1) and (2) are given in Yang et al. (2013).

To evaluate the effect of tidal energy extraction on the hydrodynamics of the system by a large commercial-scale tidal turbine farm, the maximum extractable energy of the system

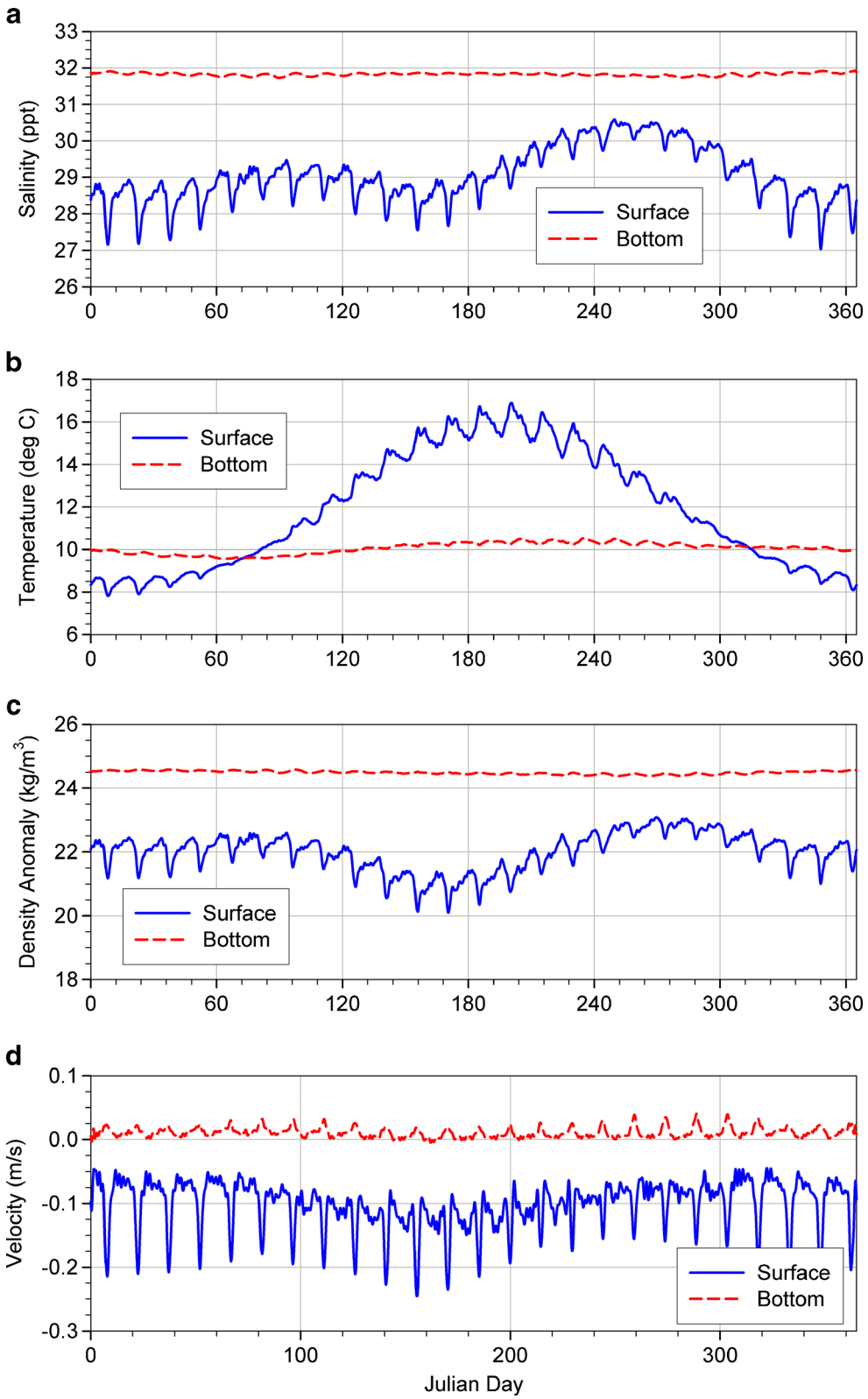

Fig. 6 Tidally averaged surface and bottom salinity (**a**), temperature (**b**), density anomaly (**c**), and velocity (**d**) at location A in the tidal channel

was first estimated. Due to high computation costs for simulating many array configurations with increasing turbine numbers, we calculated the maximum extractable energy based on simulation results for a 30-day period using the baseline model results on JD 180 as initial condition. Model simulations with tidal turbine farms were designed by deploying tidal turbines in

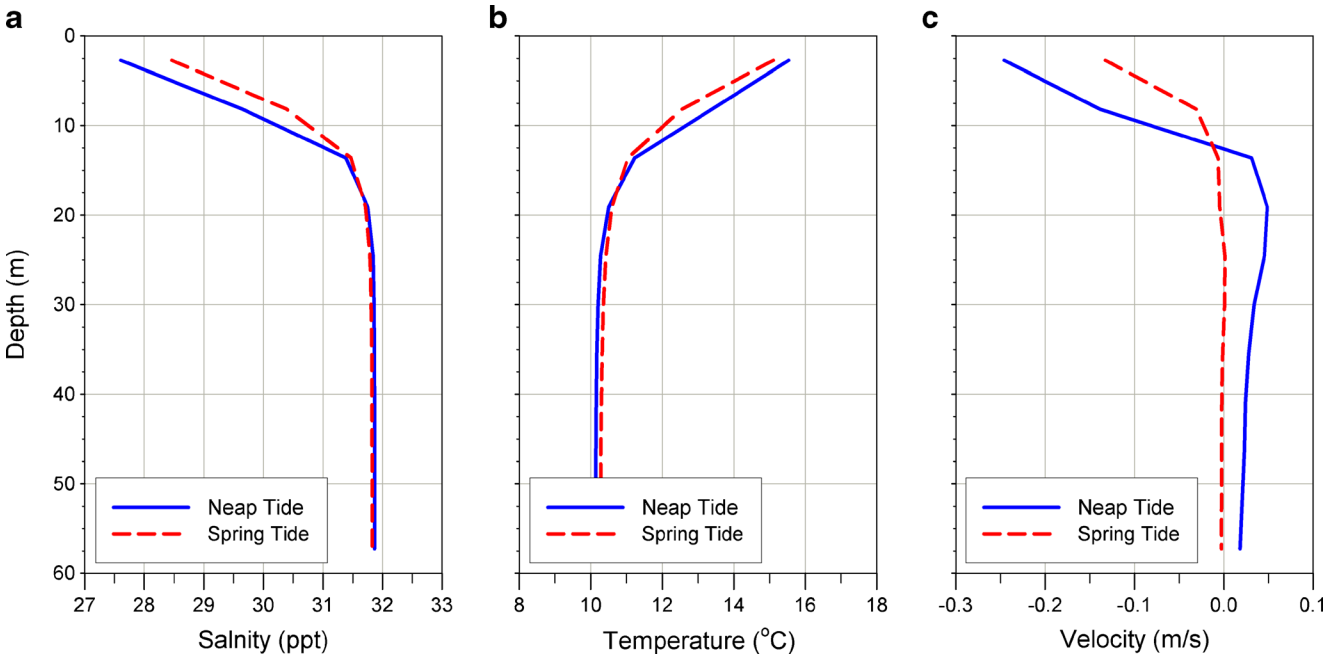

Fig. 7 Tidally averaged salinity (**a**), temperature (**b**), and velocity (**c**) profiles at location A in the tidal channel (negative velocity indicates outgoing current)

the entire channel section with increasing turbine density in each model element. The diameter of the tidal turbine was specified as 15 m, and the turbine rotor hub height was located at 10 m above the sea bed. The turbine thrust coefficient is specified as 0.5. For simplicity, effects of turbine supporting structures and turbine drag were neglected in this study.

The total extractable energy at any given time can be calculated based on the following formula (Yang et al. 2013; Sutherland et al. 2007):

$$P_{\text{total}} = \sum_{i=1}^{M} \left(N \times \frac{1}{2} \rho C_{\text{T}} A_{\text{b}} \overline{\left| \vec{u} \right|^3} \right)_i \tag{4}$$

where ρ is water density, C_{T} is the turbine thrust coefficient for the amount of thrust force exerted uniformly on a grid cell of the fluid, A_{b} is the total flow-facing area swept by turbine blades, $\vec{u}$ is the velocity vector at hub height, N is the number of turbines in each model element, and M is the total number of elements containing turbines. The tidally averaged extractable power as a function of number of turbines is plotted in Fig. 8. As the total number of turbine increases to around 17,000, the tidally averaged extractable energy reaches a maximum value of 770 MW, which is close to the total tidal energy dissipation (733 MW) in Puget Sound calculated by Lavelle et al. (1988), based on a 1-D multiply connected channel tide model with composite tidal forcing of M_2 and K_1. Model results also showed that the undisturbed tidally averaged volume flux is 2.71×10^5 m^3/s, which is also close to the value of 2.98×10^5 m^3/s obtained by Lavelle et al. (1988). The simulated instantaneous maximum volume fluxes corresponding to the undisturbed condition and maximum energy extraction condition are 5.647×10^5 and 4.096×10^5 m^3/s, respectively. Figure 8 also shows that the extractable power is approximately linearly proportional to the number of turbines, N, when N is a small percentage (e.g., <10 %) of the turbine number corresponding to the maximum extractable power.

Garrett and Cummins (2004) developed a simple analytical model to estimate the maximum extractable energy for a tidal channel connecting to a close basin, based on the tidal amplitude a outside of the channel and undisturbed volume flux Q_{max} through the channel

$$P_{\text{max}} = 0.2pgaQ_{\text{max}} \tag{5}$$

They further extended the above solution by following multiplier to include the effect of multiple tidal constituents (Garrett and Cummins 2005)

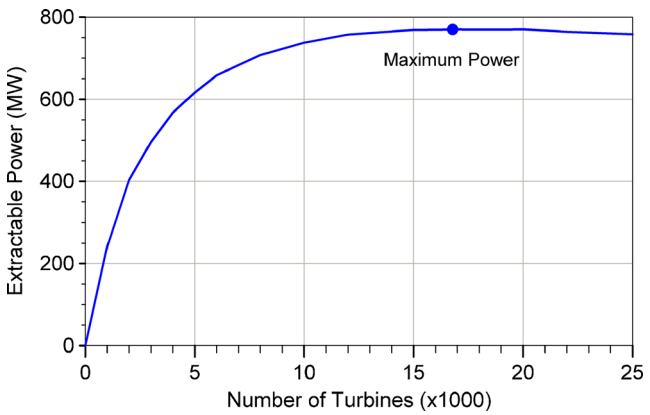

Fig. 8 Tidally averaged extractable power as a function of tidal turbines

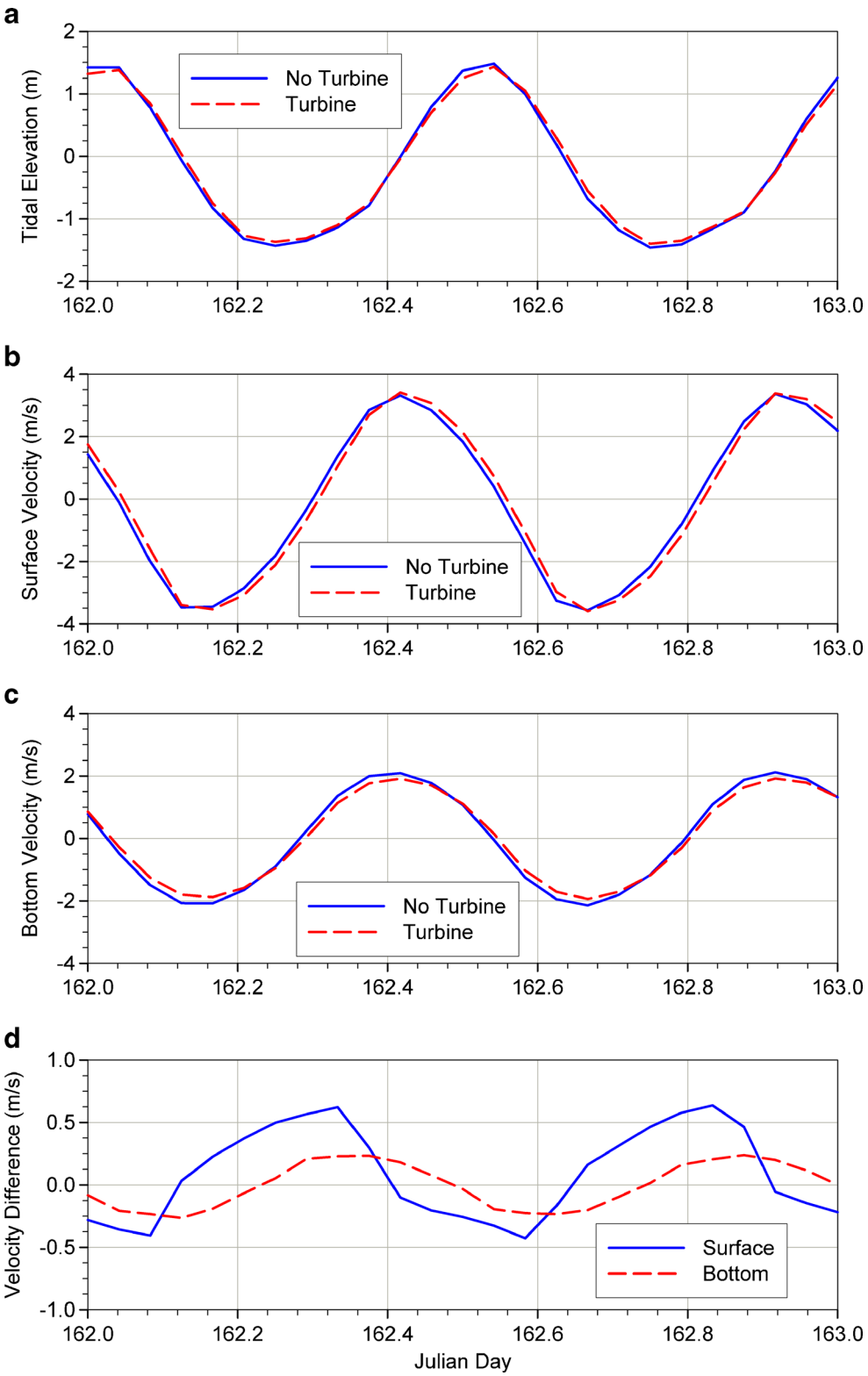

Fig. 9 Comparisons of tidal elevations (**a**) and velocities between baseline and 1,500 turbine cases at surface layer (**b**) and bottom layer (**c**) and velocity differences between baseline and 1,500 turbines cases in surface and bottom layers (**d**) at location A in the tidal channel

$$1+\left(\frac{9}{16}\right)\left[\left(\frac{a_1}{a}\right)^2+\left(\frac{a_2}{a}\right)^2+\ldots\right] \quad (6)$$

where $a_1, a_2,\ldots$ are amplitudes of additional tidal constituents. In the case of two tidal constituents, M_2 and S_2, the equation

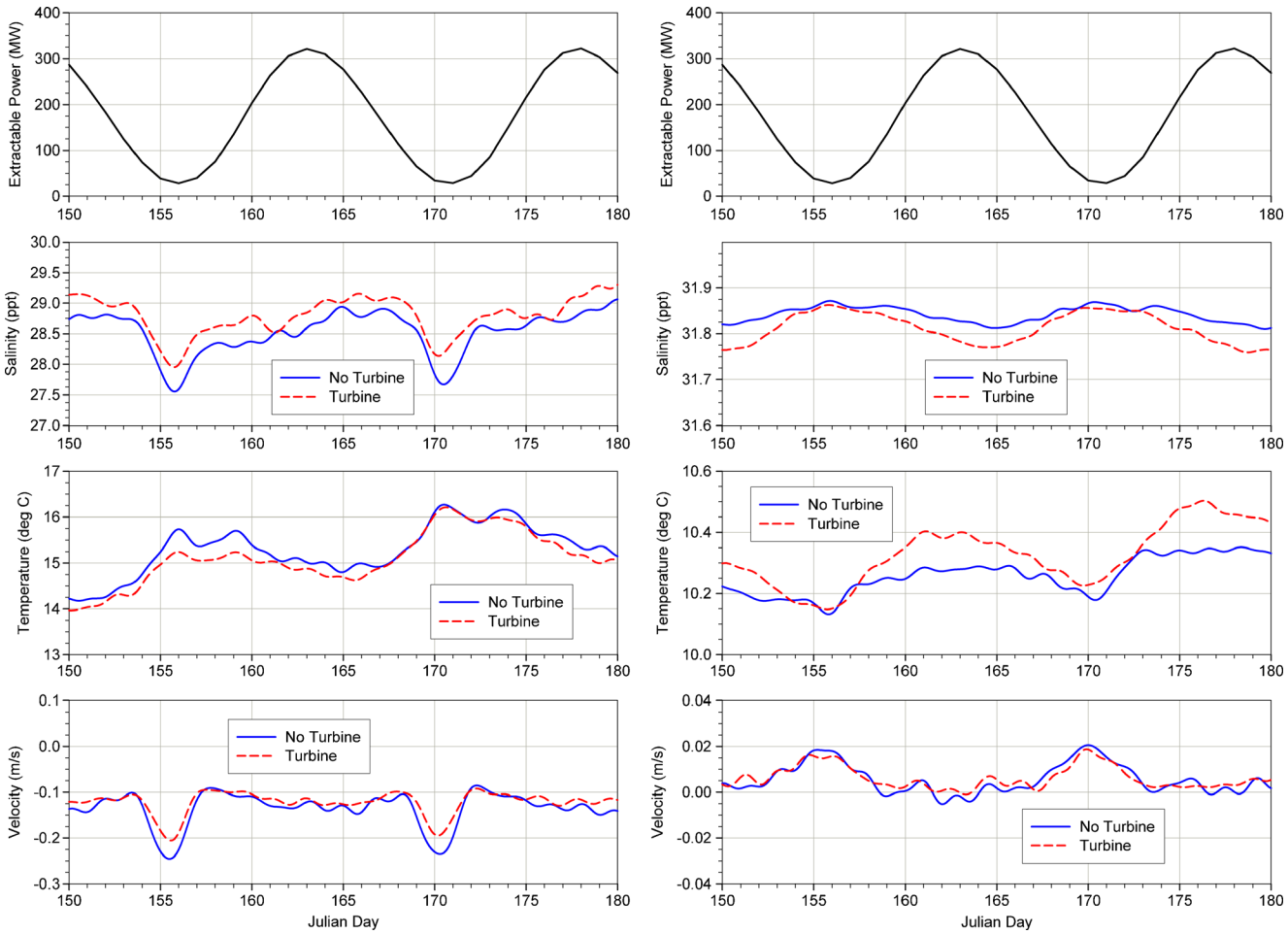

Fig. 10 Tidally averaged extractable power, surface salinity, temperature, and velocity at location A in the tidal channel between baseline and 1,500 turbines cases during the period of JD150-180 (*left panels*: surface layer; *right panels*: bottom layer)

for estimating the maximum extractable tidal energy becomes

$$P_{\max} = 0.2\rho g a_{M2}\left[1+\left(\frac{9}{16}\right)\left(\frac{a_{S2}}{a_{M2}}\right)^2\right]Q_{\max} \quad (7)$$

where a_{M2} and a_{S2} are the amplitudes of M_2 and S_2 tides, respectively. Using ρ=1,025 kg/m^2, g=9.8 m/s^2, and $Q_{\max}=5.647\times10^5$ m^3/s, a_{M2}=0.7 mand a_{S2}=0.3 m, Eq. (4) gives $P_{\max}$=870 MW, which is comparable to the model prediction of 770 MW. It should be noted that Eq. (7) was derived for the depth-average condition, and density effect was not considered. Yang et al. (2013) showed that the depth-average 2-D approach tends to overestimate the maximum extractable power than that with a 3-D approach.

Effect of Tidal Energy Extraction on Estuarine Hydrodynamics

Once the relationship between extractable power and number of tidal turbines is established and the maximum extractable power $P_{\max}$ in the system is determined (Fig. 8), we can design various array configurations to simulate the effect of tidal energy extraction by realistic commercial-scale tidal farms on the estuarine hydrodynamics. Due to the back effect of energy extraction on the flow field, the rate of extractable energy with respect to the number of tidal turbines reduces as the number of turbines increases. While many resource assessment studies were conducted to estimate the maximum extractable tidal energy (e.g., Sutherland et al. 2007; Karsten et al. 2008), extraction of all the extractable energy is not practical in the real world because it would significantly affect the marine system and require installing numerous tidal turbines. Therefore, we focused on energy extraction scenarios using a small percentage of the total tidal turbines corresponding to the maximum extractable energy.

While the large number turbines (such as 17,000 shown in Fig. 8) for generating the maximum power is unrealistic, it is possible to extract tidal energy for a tidal farm with a much less number of turbines, for instance, a small percentage of the maximum 17,000 turbines. Three model simulations were conducted, with three different sizes of turbine arrays. The

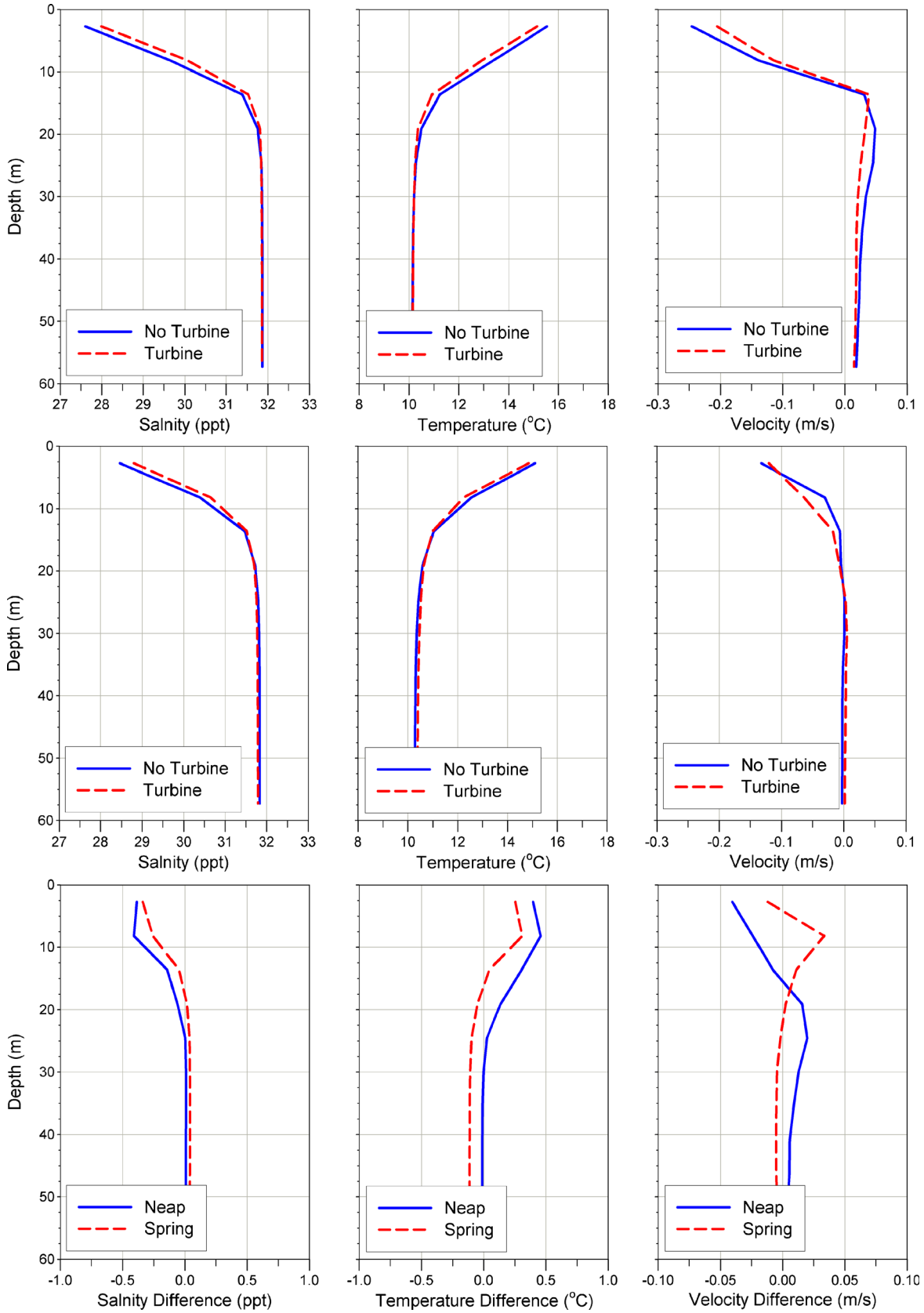

Fig. 11 Comparisons of tidally averaged salinity, temperature, and velocity profiles between baseline and 1,500 turbine cases at location A in the tidal channel. *Upper panels*: neap tide (JD156). *Middle panels*: spring tide (JD163). *Lower panels*: differences between baseline and 1,500 turbines cases at spring and neap tides

largest array has 1,500 tidal turbines, which is about 9 % of the total turbines (around 17,000 turbines) for generating the maximum extractable tidal energy. The other two arrays consist of 400 and 800 turbines, respectively, which correspond to about 2.4 and 5 % of the total turbines for generating the maximum extractable tidal energy. For the purpose of better visualizing the effect of energy extraction, model results for the scenario with 1,500 turbines and a hub height of 10 m were first analyzed and compared to the baseline condition. The turbine array occupies the entire cross section (3,000 m in width) of the tidal channel for a section 13,000 m long, which results in a total coverage area of 39×10^6 m^2. This configuration is equivalent to one turbine per 26,000-m^2 area or approximately 200 m apart in the transverse direction and 130 m apart in the longitudinal direction between turbines. A thrust coefficient of 0.5 was used in the simulation.

Comparisons of tidal elevations and tidal currents at the tidal channel between the 1,500 turbines scenario and baseline condition (no turbine) during spring tide (JD 163) are shown in Fig. 9. We can see that the effect of tidal energy extraction with 1,500 turbines on the tidal elevation is relatively small (Fig. 9a). The maximum tidal flood (positive) and ebb (negative) currents in the surface layer are nearly the same between the turbine scenario and baseline condition (Fig. 9b). However, there is a phase lag in the surface velocity for the turbine scenario with respect to the baseline condition because of additional drag induced by the turbines. In the bottom layer, the maximum flood and ebb currents in the turbine scenario are smaller than those in the baseline condition because the bottom layer is close to the turbine hub height, and velocities are directly affected by the energy extraction. Similar to surface currents, a phase lag is also seen in the bottom velocities (Fig. 9c). Velocity differences between baseline condition and turbine scenario in surface and bottom layers are shown in Fig. 9d. The greatest difference in the surface velocities occurs during slack tides when currents start to reverse directions. During flood and ebb tides when surface tidal currents become strongest, velocity differences in the surface layer are close to zero. In contrast, the largest differences in the bottom layer velocities between turbine and baseline conditions occur near flooding and ebbing phases when tidal current and extractable energy are greatest.

Tidally averaged estuarine stratification and circulation play an important role in water exchange and transport processes in estuaries and bays. As shown in Fig. 6, tidally averaged salinity, temperature, and velocity have strong fortnightly modulations and long-term seasonal variations. Comparisons of mean salinity, temperature, and velocity between baseline and turbine conditions were made for the period of JD 150 to JD 180 (Fig. 10), when the two-layer estuarine circulation is greatest as a combined result of high river inflow and warm surface water temperature (Fig. 6). For reference, the tidally averaged extractable energy was also plotted in the top panel of Fig. 10. During neap tides (JD 156 and JD171) when tidal currents and mixing are weakest (thus, the extractable energy is smallest), a sharp decrease in salinity and an increase in temperature are seen in the surface layer (Fig. 10, left panel), and a small increase in salinity and decrease in temperature are also seen in the bottom layer (Fig. 10, right panel). As a result, stronger two-layer circulation also occurs during neap tides, i.e., tidally averaged velocities in opposite directions at the surface and bottom become stronger. Tidally averaged salinity under turbine scenario is reduced in the surface layer and increased in the bottom layer, as a result of the increase of vertical mixing due to tidal energy extraction. Note that the change of salinity in the surface layer is almost an order of magnitude larger than that in the bottom. Similarly, tidally averaged temperature is reduced in the surface layer and increased in the bottom layer (during warm season) under turbine scenario. Extraction of tidal energy thus also reduces the two-layer estuarine circulation, especially during neap tides when tidal mixing is weakest and stratification is strongest in the estuary. It is important to point out that although the extractable tidal energy is stronger in spring tide than in neap tide because it is directly proportional to the cube of the tidal velocity magnitude (Eq. 4), the effect of tidal energy extraction on the fortnightly variability of estuarine circulation is stronger during neap tide than spring tide, a phenomenon similar to the effect of shallow sill on fjord circulation reported by Geyer and Cannon (1982).

Vertical profiles of tidally averaged salinity, temperature, and velocity during neap (JD156) and spring (JD163) tides are shown in Fig. 11 (upper and middle panels). Comparisons between baseline and turbine conditions clearly show that extraction of tidal energy would increase the surface salinity and decrease the surface temperature, thus reducing the vertical stratification and the estuarine two-layer circulation, especially during neap tides. The differences of vertical profiles between the baseline and turbine conditions are shown in the lower panel of Fig. 11. Overall, tidal energy extraction has stronger impact on the tidally averaged salinity, temperature, and velocity in the surface layer and neap tides than those in the bottom layer and spring tides.

Effect of Different Array Configurations

To further examine the effects of tidal energy extraction on the estuarine hydrodynamics with different array configurations, two additional simulations were conducted. The detailed array configurations for all the simulations are listed in Table 2. Turbine blade diameter and thrust coefficient remain the same, 15 m and 0.5, in all the model runs. The additional model runs were designed to simulate a smaller and more practical number of tidal turbines (400 and 800). The 400- and 800-turbine scenarios occupy a slightly smaller region (36×10^6 m^2) than the 1,500-turbine scenario (39×10^6 m^2). The 400-turbine scenario has a lateral turbine spacing of 300 m and a

Table 2 Array configurations

Total turbine	Coverage area (m^2)	Lateral spacing (m)	Longitudinal spacing (m)	Blade diameter (m)	Hub height (m)
1,500	39×10^6	200	130	15	10
800	36×10^6	300	150	15	10
400	36×10^6	300	300	15	10

longitudinal spacing of 300 m, respectively (see the inset image in Fig. 1). The 800-turbine scenario has a lateral turbine spacing of 300 m but a longitudinal spacing of 150 m, which is half of the distance in the 400-turbine scenario.

Time series of tidally averaged extractable energy during JDs 150–180 for all three scenarios listed in Table 2 are shown in Fig. 12. The maximum tidally average powers at spring tide for 400, 800, and 1,500 turbines with 10-m hub height scenarios are 115, 210, and 312 MW, which correspond to the extractable power per unit turbine of 288, 262, and 208 KW, respectively. Therefore, the extractable power output per unit turbine reduces as the number of turbines increases (as shown in Fig. 8) but remains approximately constant when the number of turbines is much smaller than the total number of turbines that corresponds to the maximum extractable energy in the system.

To evaluate the effects of energy extraction on the stratification and estuarine circulation under different array configurations, differences (surface value minus bottom value) of surface and bottom tidally averaged salinities, temperatures, and velocities during spring and neap tides are plotted and compared in Fig. 13. Zero turbine number represents the baseline condition. As seen in Fig. 13, stratification and two-layer circulations in neap tide are consistently stronger than those in spring tide. For all the scenarios, differences of surface and bottom salinities and temperatures decrease as the number of turbines increases. Differences of surface and bottom mean velocities show the same decreasing trend during neap tide while remain nearly the same during spring tide.

Summary

The effect of tidal energy extraction on stratification and baroclinic circulation has been studied in the past. In this study, an unstructured-grid coastal ocean model FVCOM with a tidal turbine module was applied to simulate the effect of tidal energy extraction on the stratification and two-layer estuarine circulation in a stratified estuarine system, which consists of a tidal basin with river discharge and a narrow tidal channel connecting to the open coastal water. The full annual cycle with seasonal variability of stratification and two-layer estuarine circulation was simulated with forcing of tide, river inflow, and meteorological heat flux. Numerical model runs for tidal energy extraction were conducted by deploying a fence of tidal turbines in the tidal channel. Although there has not been any commercial-scale tidal farm installed in a real site, it is expected that a tidal power farm with hundreds of turbines and even up to a thousand can be developed in a large site, such as Alderney Race of the UK (Myers and Bahaj 2005; Neill et al. 2012), over the next decade. To realistically represent a commercial-scale tidal farm, three different arrays with a total number of tidal turbines of 400, 800, and 1,500 were considered in the model simulations; all were within the 10 % limit of the total number of turbines corresponding to the maximum extractable energy in the system. Results from this study could be used as a reference for future studies on the effect of tidal energy extraction as well as guidance by industry for environmental impact assessment during planning stage.

Model results show that extraction of tidal energy with a turbine hub height close to the bottom layer of the water column not only reduces the bottom tidal current but also results in a

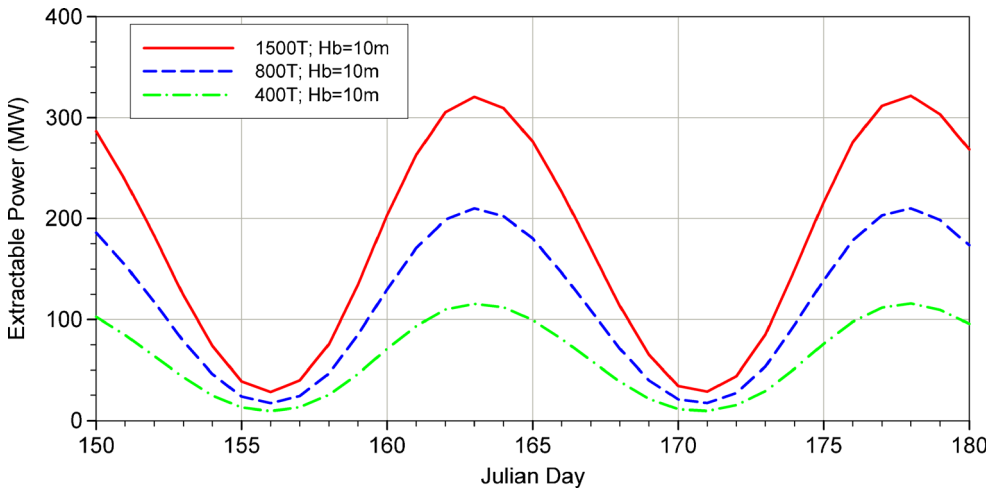

Fig. 12 Tidally averaged extractable powers under different turbine array configurations

phase shift. The main effect of energy extraction on the surface tidal current is the phase shift, which results in a larger velocity difference between the conditions with and without tidal turbines than that in the bottom layer because surface velocity is much greater than the bottom velocity. Tidal energy extraction will increase the vertical mixing and weaken the stratification and two-layer circulation in the estuary. Although tidal energy extraction is highest during spring tides when the tidal currents are strongest, the effect on the tidally averaged two-layer circulation is greatest during neap tides because of the changes in vertical mixing and stratification in neap tides. The effect on the two-layer circulation is small during spring tides, mainly because of the strong tidal mixing. Our model results show that for a small number of turbines, such as <10 % of the total number of turbines for the maximum extractable energy, the effect of tidal energy extraction on stratification and baroclinic flow is relatively small. However, as reported in previous studies (Garrett and Cummins 2005; Sutherland et al. 2007; Yang et al. 2013), the total volume flux (barotropic flow) across the channel would be reduced at a higher rate for a smaller number of turbines.

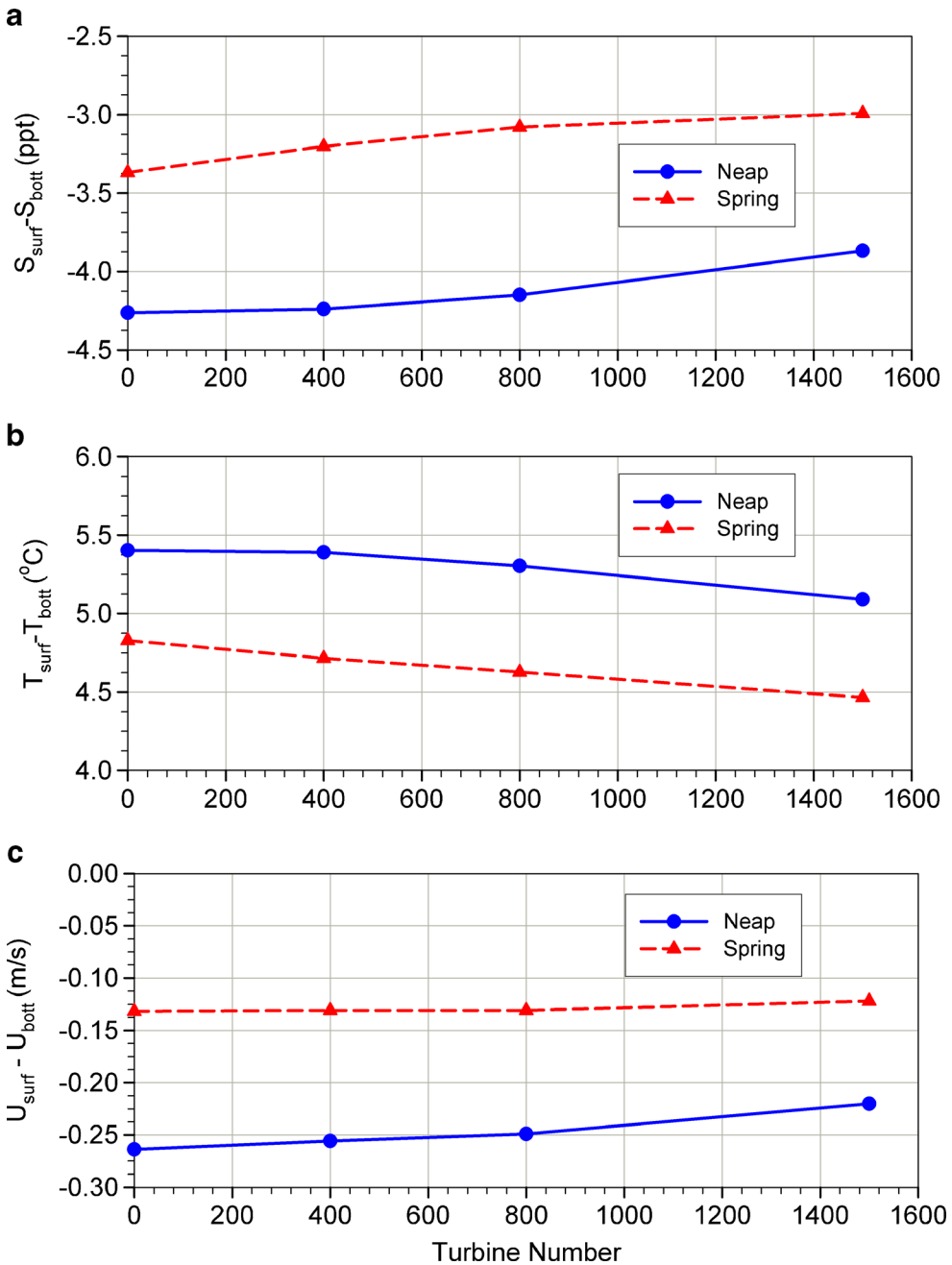

Fig. 13 Differences of surface and bottom tidally averaged salinities (**a**), temperatures (**b**), and velocities (**c**) at location A in the tidal channel for different array configurations during neap tide (JD 156) and spring tide (JD 163)

Therefore, it is important to keep in mind that the effect of tidal energy extraction on physical processes in marine environment should be considered for both baroclinic and barotropic flow conditions. The effect of tidal energy extraction on stratification and estuarine circulation would have implication to the long-term biogeochemical processes in estuaries because of the potential change of flushing time in the system.

While this study provides interesting and important results for assessing the impacts of tidal energy extraction on estuarine hydrodynamics, such as mixing, stratification, and two-layer circulation, many issues remain for further investigation. For example, how do the changes in barotropic and baroclinic motions due to tidal energy extraction interact and affect the overall transport processes in the estuary? What is the cost and benefit of energy extraction with a larger number of turbines due to the effect on the environment and the decrease of power output rate as the total extractable power is increased? While our study shows that the greatest impact of energy extraction occurs during neap tides, what would be the change of impact during neap tide if turbines were shut off during neap tides when tidal currents are weakest? Finally, it is important to apply the model in a real-world case and further evaluate the impacts and confirm the findings obtained in this study.

Acknowledgments This study is funded by the Wind and Water Power Program under the Office of Energy Efficiency and Renewable Energy, U.S. Department of Energy. The authors thank Dr. Andrea Copping for discussion throughout this study.

References

Ahmadian, R., R. Falconer, and B. Bockelmann-Evens. 2012. Far-field modelling of the hydro-environmental impact of tidal stream turbines. *Renewable Energy* 38: 107–116.

Blanchfield, J., C. Garrett, P. Wild, and A. Rowe. 2008. The extractable power from a channel linking a bay to the open ocean. *Proceedings of the Institution of Mechanical Engineers, Part A: Journal of Power and Energy* 222: 289–297.

Chen, C., H. Liu, and R.C. Beardsley. 2003. An unstructured, finite-volume, three-dimensional, primitive equation ocean model: application to coastal ocean and estuaries. *Journal of Atmospheric and Oceanic Technology* 20: 159–168.

Cole, T.M., and S.A. Wells. 2009. CE-QUAL-W2: a two-dimensional, laterally averaged, hydrodynamic and water quality model, version 3.6 user manual. Instruction Report EL-08-1, U.S. Army Corps of Engineers, Washington, DC 20314–1000.

Defne, Z., Haas, K.A., Fritz, H.M. 2011. Numerical modeling of tidal currents and the effects of power extraction on estuarine hydrodynamics along the Georgia coast USA. Renewable Energy 36:3461–3471. doi:10.1016/j.renene.2011.05.027.

Draper, S., G. Houlsby, M. Oldfield, A. Borthwick. 2009. Modeling tidal energy extraction in a depth-averaged coastal plain. Proceedings of the 8th European Wave and Tidal Energy Conference, Uppsala, Sweden

Garrett, C., and P. Cummins. 2004. Generating power from tidal currents. *Journal of Waterway Port Coastal and Ocean Engineering* 130: 114–118.

Garrett, C., and P. Cummins. 2005. The power potential of tidal currents in channels. *Proceedings of the Royal Society of London A* 461: 2563–2572.

Garrett, C., and P. Cummins. 2008. Limits to tidal current power. *Renewable Energy* 33: 2485–2490.

Geyer, W.R., and G.A. Cannon. 1982. Sill processes related to deep water renewal in a fjord. *Journal of Geophysical Research* 87(C10): 7985–7996. doi:10.1029/JC087iC10p07985.

Geyer, W.R., R. Chant, and R. Houghton. 2008. Tidal and spring-neap variations in horizontal dispersion in a partially mixed estuary. *Journal of Geophysical Research* 113, C07023. doi:10.1029/2007JC004644.

Hasegawa, D., J. Sheng, D.A. Greenburg, and K.R. Thompson. 2011. Far-field effects of tidal energy extraction in the Minas Passage on tidal circulation in the Bay of Fundy and Gulf of Maine using a nested-grid coastal circulation model. *Ocean Dynamics* 61: 1845–1868. doi:10.1007/s10236-011-0481-9.

Huang, H., C. Chen, J.O. Blanton, and F.A. Andrade. 2008. Numerical study of tidal asymmetry in the Okatee Creek. *South Carolina Estuaries Coastal and Shelf Science* 78: 190–202.

Karsten, L.K., J.M. McMillian, M.J. Lickley. 2008. Assessment of tidal current energy in Minas Passage, Bay of Fundy. Proc IMechE, Part A: Journal of Power Energy. 222:493–507.

Lavelle, J.W., H.O. Mojfield, E. Lempriere-Doggett, G.A.Cannon, D.J. Pashinski, E.D. Cokelet, L. Lytle, and S. Gill. 1988. A multiple connected channel model of tides and tidal currents in Puget Sound, Washington, and a comparison with updated observations. NOAA Technical Memorandum ERL PMEL-84, 108 pp.

Myers, L., and A.S. Bahaj. 2005. Simulated electrical power potential harnessed by marine current turbine arrays in the Alderney Race. *Renewable Energy* 30: 1713–1731.

Murphy, P.L., and Valle-Levinson. 2008. Tidal and residual circulation in the St. Andrew Bay system, Florida. *Continental Shelf Research* 28: 2678–2688.

Neill, S.P., E.J. Litt, S.J. Couch, and A.G. Davies. 2009. The impact of tidal stream turbines on large-scale sediment dynamics. *Renewable Energy* 38: 107–116.

Neill, S., J.R. Jordan, and S.J. Couch. 2012. Impact of tidal energy converter (TEC) arrays on the dynamics of headland sand banks. *Renewable Energy* 37: 387–397.

Qi, J.C., Chen, R.C., Beardsley, W. Perrie and G. Cowles. 2009. An unstructured-grid finite-volume surface wave model (FVCOM-SWAVE): implementation, validations and applications. *Ocean Modelling* 28: 153–166. doi:10.1016/j.ocemod.2009.01.007.

Shapiro, G. 2010. Effect of tidal stream power generation on the region-wide circulation in a shallow sea. *Ocean Science Discussions* 7: 1785–1810.

Sutherland, G., M. Foreman, and C. Garrett. 2007. Tidal current energy assessment for Johnstone Strait, Vancouver Island. *Proceedings of the Institution of Mechanical Engineers, Part A. Journal of Power and Energy* 221(A2): 147–157.

Sun, X., J. Chick, and I. Bryden. 2008. Laboratory-scale simulation of energy extraction from tidal currents. *Renewable Energy* 33: 1267–1274.

Walkington, I., and R. Burrows. 2009. Modeling tidal stream power potential. *Applied Ocean research* 31: 239–245.

Weisberg, R.H., and L. Zheng. 2006. Circulation of Tampa Bay driven by buoyancy, tides, and winds, as simulated using a finite volume coastal ocean model. Journal of Geophysical Research Oceans. 111:C01005. doi:10.1029/2005JC003067.

Xue, P., C. Chen, P. Ding, R.C. Beardsley, H. Lin, J. Ge, and Y. Kong. 2009. Saltwater intrusion into the Changjiang River: a model-guided mechanism study. *Journal of Geophysical Research* 114, C02006. doi:10.1029/2008JC004831.

Yang, Z., K.L. Sobocinski, D. Heatwole, T. Khangaonkar, R. Thom, and R. Fuller. 2010. Hydrodynamic and ecological assessment of nearshore restoration: a modeling study. *Ecological Modelling* 221(1043): 1053. doi:10.1016/j.ecolmodel.2009.07.011.

Yang, Z., and T. Khangaonkar. 2010. Multi-scale modeling of Puget Sound using an unstructured-grid coastal ocean model: from tide flats to estuaries and coastal waters. *Journal of Ocean Dynamics* 60: 1621–1637. doi:10.1007/ZJQ13590088661.

Yang, Z., T. Wang, T. Khangaonkar, and S. Breithaupt. 2011. Integrated modeling of flood flows and tidal hydrodynamics over a coastal floodplain. *Environmental Fluid Mechanics*. doi:10.1017/BM-13702733717.

Yang, Z. and T. Wang, 2013. Tidal residuals, eddies and their effects on water exchange in puget sound. *Ocean Dynamics* 63: 995-1009. doi:10.1007/s10236-013-0635-z.

Yang, Z., T. Wang, and A. Copping. 2013. Modeling tidal stream energy extraction and its effects on transport processes in a tidal channel and bay system using a three-dimensional coastal ocean model. *Renewable Energy* 50: 605–613. doi:10.1016/j.renene.2012.07.024.